



HAL
open science

Correlation between mechanical and structural properties as a function of temperature within the $\text{TeO}_2\text{-TiO}_2\text{-ZnO}$ ternary system

J. de Clermont-Gallerande, Maggy Colas, F. Celarie, Y. Gueguen, M. Bergler, D. de Ligny, T. Hayakawa, P. Thomas

► To cite this version:

J. de Clermont-Gallerande, Maggy Colas, F. Celarie, Y. Gueguen, M. Bergler, et al.. Correlation between mechanical and structural properties as a function of temperature within the $\text{TeO}_2\text{-TiO}_2\text{-ZnO}$ ternary system. *Journal of Non-Crystalline Solids*, 2020, 528, pp.119716. 10.1016/j.jnoncrysol.2019.119716 . hal-03063712

HAL Id: hal-03063712

<https://hal.science/hal-03063712>

Submitted on 14 Dec 2020

HAL is a multi-disciplinary open access archive for the deposit and dissemination of scientific research documents, whether they are published or not. The documents may come from teaching and research institutions in France or abroad, or from public or private research centers.

L'archive ouverte pluridisciplinaire **HAL**, est destinée au dépôt et à la diffusion de documents scientifiques de niveau recherche, publiés ou non, émanant des établissements d'enseignement et de recherche français ou étrangers, des laboratoires publics ou privés.

Correlation between mechanical and structural properties as a function of temperature within the TeO₂-TiO₂-ZnO ternary system.

J. de Clermont-Gallerande¹ ; M. Dutreilh-Colas¹ ; F. Célarie² ; Y. Gueguen² ; M. Bergler³ ; D. de Ligny³ ; T. Hayakawa⁴ ; P. Thomas¹

¹Institut de recherche sur les céramiques (IRCER), UMR 7315 CNRS / Université de Limoges, Centre Européen de la Céramique, 12, rue Atlantis, 87068 Limoges, France

² Institut de Physique de Rennes (IPR), UMR6251 CNRS, Université de Rennes, 263 Avenue Général Leclerc, 35700 Rennes, France

³ Institute of Glass and Ceramics, DMSE, University of Erlangen-Nuremberg, DE 91058 Erlangen, Germany

⁴Field of Advanced Ceramics, Department of Life Science and Applied Chemistry / Frontier Research Institute of Materials Science (FRIMS), Nagoya Institute of Technology, Gokiso, Showa, Nagoya 466-8555, Japan

Abstract

In situ Raman spectroscopy, Resonance Frequency and Damping Analysis (RFDA) setup and Associated Raman Brillouin Calorimeter (ARABICA) setup experiments as a function of temperature were conducted on the (100-x)TeO₂-5TiO₂-xZnO (x=15; 17.5; 20; 22.5; 25) glass system. Structural and mechanical properties showed non-conventional properties evolution as a function of ZnO content which are managed by the modification of ZnO polyhedra. Before glass transition temperature (T_g), the evolution of the Boson peak (BP) frequencies and the elastic properties are in accordance with the idea of the relaxation of the strains inside the glass; after T_g, their evolution shows the transition toward a viscous liquid. BP and mechanical properties study evidences that as nano-heterogeneous domains size increases at a faster rate, the mechanical properties will decrease at a slower rate. This point will be helpful for choosing appropriate composition for optical fiber shaping.

Introduction

Tellurite glasses have interested researchers in the field of photonic application for many years. Indeed, they are good candidates for optical fibers thanks to their high linear refractive index, high dielectric constant, wide infrared transmittance, and their high third order non-linear optical values (1–4).

Ab-initio studies showed that the pure TeO₂ glasses have the highest non-linear optical properties among tellurite glasses (5) (fifty times more than fused silica glasses (4,6)), but extreme quenching conditions are needed to obtain glass (7). Consequently, modifier oxides are required. Different systems have been studied in their abilities to form glasses (glassy domains) and their structural, linear and non-linear optical properties for many years in IRCER laboratory (8–14). Among them, adding TiO₂ is well known to increase the glass forming ability resulting in homogeneous glasses with only slight changes in the structure of pure TeO₂ glass (8,15,16).

Adding ZnO in tellurite glasses significantly increases the glass forming domain (up to 40mol% ZnO) (17). Binary TeO₂-ZnO glasses are useful media for ultra-low loss optical fibers (1 dB/km) in the wavelength range of 3.4-4 μm (18). Different studies have been done on TeO₂-ZnO glasses based on Raman spectroscopy data (19–23), and neutron and X-ray diffraction

45 (24). The different studies showed that adding ZnO to the original TeO₂ glass matrix results in
 46 (i) a structural transformation of TeO₄ into TeO₃ units and so a linear decrease of the optical
 47 properties (ii) a band gap decrease as the glasses turn more transparent upon adding ZnO (25).

48 The goal of the present study is to highlight a correlation between the evolution of the
 49 mechanical properties and the structure of (100-x)TeO₂-5TiO₂-xZnO (x=15, 17.5, 20, 22.5, 25
 50 (TTZ) glasses as a function of temperature especially around the glass transition temperature
 51 (T_g). In this study, the medium-range structure of TTZ glasses is studied using in-situ Raman
 52 spectroscopy and mechanical properties by Resonance Frequency and Damping Analysis
 53 (RFDA) and Brillouin experiments (26). By looking at the properties of the glass as a function
 54 of temperature, it might be possible to have an idea of their ability to fiber shaping..

55 1. Experimental

56 1.1. Sample preparation

57 The relevant amount of the different initial powders (commercial: α-TeO₂: Toldini 99,9%,
 58 TiO₂: Aldrich 99%, ZnO : Alfa Aesar 99,99%) within the ternary system (100-x)TeO₂-5TiO₂-
 59 xZnO % mol, with x= 15; 17.5; 20; 22.5 and 25 (respectively named TTZ15, TTZ17.5, TTZ20,
 60 TTZ22.5 and TTZ25) were ground in a mortar then melted in a platinum crucible at 850°C
 61 before being quenched on a brass mold preheated at 150°C. The glass domain is smaller than
 62 the one found in (25) due to the amount of powder used (13g) to synthesize the samples for
 63 mechanical experiment. The obtained glasses were then annealed at 30°C below the glass
 64 transition temperature (taken from (25,27)) for 12 hours in order to release stresses resulting
 65 from the melt-quenching method. The final concentrations of the samples have been controlled
 66 by EDS experiments which evidence a deviation less than 2% from the theoretical composition.

67 As many experiments have been done, the size and synthesis conditions of the samples have
 68 been adapted to the needs of each measure. All the relevant information are summarized in the
 69 Table 1.

Experiment	Initial mass (g)	Melting time (h)	Ground or polished	Form of the sample	Sample size (mm)
Raman spectroscopy	2	1	Ground	Powder	N/A
RFDA	13	5	Polished	Parallelepiped	l=30
					L=15
					e=3
ARABICA*	2	1	Polished	Cylinder	D=3
					h=1

70 *Table 1 : Information on the different experimental procedures for each experiment. *Associated Raman,*
 71 *Brillouin Calorimetry. D: diameter; h: height of a cylinder; l: length of a parallelepiped; L: width of a*
 72 *parallelepiped; e: thickness of a parallelepiped.*

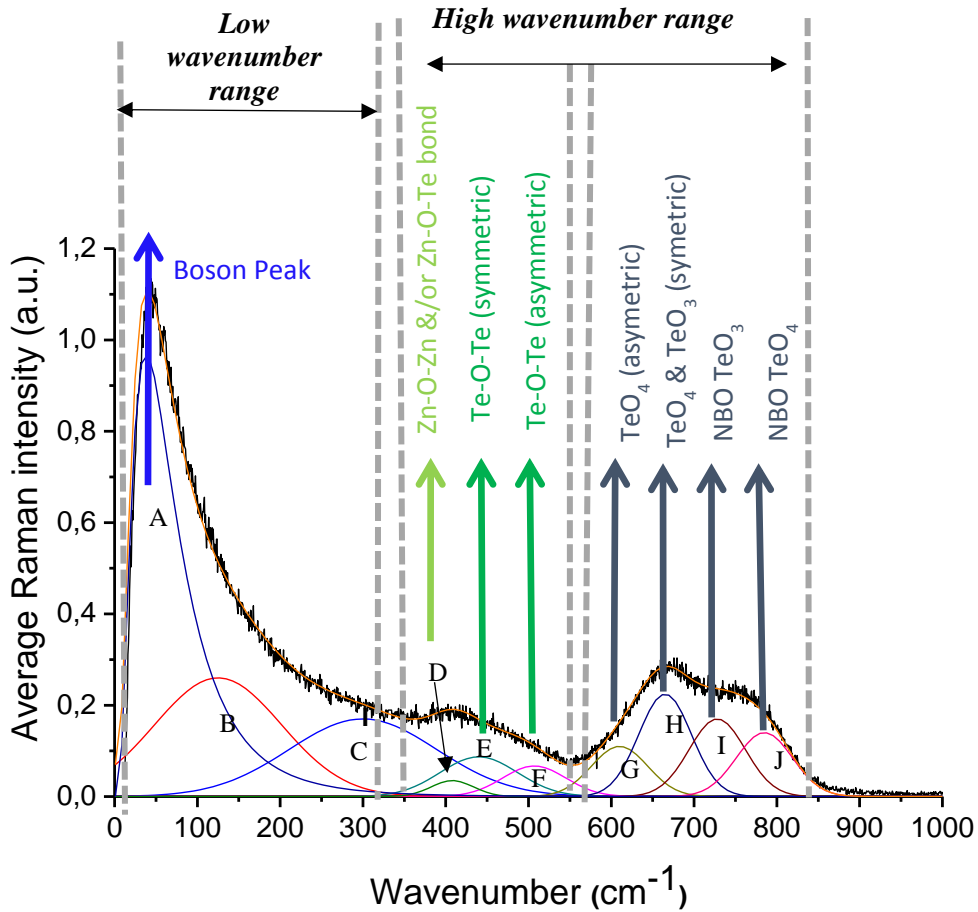
73 Raman spectra were recorded in the 10-1000cm⁻¹ spectral range, using a T64000 HORIBA
 74 Jobin-Yvon spectrometer operating in the triple subtractive configuration at 514.5 nm. Samples
 75 were heat using a LINKAM TMS600 device (5°C/minute).

76 All Raman spectra were normalized (total area normalization) and baseline corrected (linear
 77 correction).

78 The normalized spectra were then decomposed using the Focus program (28) based on
 79 previous studies (10,25,29), with 10 oscillators: 9 Gaussian functions and 1 log-normal
 80 function. As the spectra are recorded at different temperature, all functions were independently

81 corrected from the Bose-Einstein factor. Due to the width and overlapping of the bands of the
 82 normalized Raman spectra (figure 1) all Gaussian functions were width at half maximum
 83 (FWHM) and frequency fixed, and only the intensity was left free. As the log-normal function
 84 is well defined, all fitting parameters were left totally free (frequency, FWHM and intensity).

85 The TTZ glass Raman spectra's frequencies range can be divided in two different parts: the
 86 low wavenumber region with the Boson peak (BP), the high wavenumber region (300-800 cm^{-1})
 87 with the deformation of bridges (Zn-O-Zn or Zn-O-Te and asymmetric and symmetric Te-O-
 88 Te) and the elongation vibrations of Te-O bonds for TeO_3 and TeO_4 polyhedra (figure 2).



89

90 *Figure 1 : Raman bands attribution of a typical TTZ sample (Example of the TTZ15 sample)*

91

92 The mechanical properties have been obtained by Resonance Frequency and Damping
 93 Analysis (RFDA). Details on this technique can be found in the ASTM international base (26).
 94 Sample have been heat until the loss of the signal (10°C/minute).

95 Brillouin measurements have been done on the ARABICA platform (Associated Raman
 96 Brillouin Calorimetry) (30). Samples have been heated at 10°C/min until 420°C. Time
 97 accumulation from Brillouin signal is 30 seconds (spectrum each 5°C).

98 2. Results and discussion

99 2.1. Raman spectroscopy

100 Vibrational studies of TeO_2 -ZnO glasses have been extensively done (19–21) at room
 101 temperature. It has been reported (20) that adding ZnO in the glasses has different

102 consequences. By Raman spectroscopy, a shift of the band corresponding to the vibration of
103 the TeO_4 polyhedra toward higher frequencies and a shift of the band corresponding to the
104 vibration of the non-bridging oxygen in TeO_3 and TeO_4 polyhedra to higher values
105 accompanied by a progressive increase in intensity are observed. A decrease of the intensity of
106 the band corresponding to the vibration of the Te-O-Te bridges and a shift to lower frequencies
107 is also noted.

108 According to *Bürger et al.* (20), it has been evidenced that the introduction of zinc oxide in
109 TeO_2 glasses will induce Non Bridging Oxygens (NBO) species. The length of one of the Te-
110 O bond of the TeO_4 units gradually increase, leading into TeO_{3+1} units and then TeO_3 units with
111 an increase in zinc oxide content.

112 *Kozukharov et al.* reported that ZnO is introduced as ZnO_6 octahedra either within tellurite
113 chains or between them (23). At low content of ZnO, a part of the TeO_4 trigonal bipyramids
114 (tbps) becomes asymmetric, producing TeO_{3+1} units observed in the $\text{Zn}_2\text{Te}_3\text{O}_8$ crystalline
115 phase. For higher concentration of ZnO, the TeO_{3+1} units loose one oxygen to become TeO_3
116 trigonal pyramids (tp) found in ZnTeO_3 crystalline phase (23).

117 *Thorbahn et al.* (24), evidenced by Raman spectroscopy and EXAFS experiments for binary
118 TeO_2 -ZnO glasses that Zn coordination number decreases from 6 ± 1.6 to 4 ± 0.6 with a Zn-O
119 bond length that remained constant with increasing ZnO content. It was also reported that rather
120 than the ZnO_6 configuration discussed above, ZnO is present in the form of ZnO_4 tetrahedra for
121 high ZnO content (24).

122 In a previous study in IRCER laboratory, *Ghribi et al.* have studied the TeO_2 - TiO_2 -ZnO and
123 the TeO_2 - GeO_2 -ZnO system at room temperature (25,29). They concluded that adding ZnO in
124 glassy matrix will in a first step lead to breaking Te-O-Te bridges, including network
125 depolymerization, and in a second step, with more ZnO content, to the formation of Te-O-Zn
126 and Zn-O-Zn bridges.

127 As the role of ZnO is still unclear, we proposed here a structural investigation of the ternary
128 system TTZ on a wide ZnO range content (15-25 mol%) from RT up to crystallization
129 temperature. However, the crystallization of the samples won't be discuss in this paper.

130 Nevertheless, as parent crystallized phases give good indications of the unit, which can be
131 evidence in glasses, an overview of crystallized phases in the TeO_2 -ZnO binary system is
132 proposed.

133 Two stable crystalline phases respectively ZnTeO_3 for 50% mol TeO_2 - 50% mol ZnO and
134 $\text{Zn}_2\text{Te}_3\text{O}_8$ for 60% mol TeO_2 -40% mol ZnO (31,32) can be found (33).

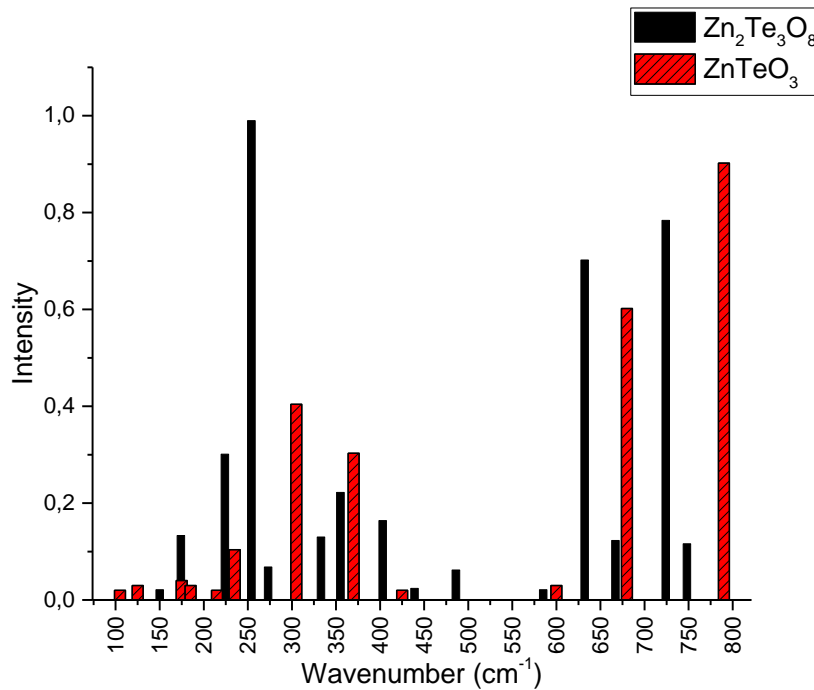
135 The $\text{Zn}_2\text{Te}_3\text{O}_8$ structure is composed of chain-like structure with Te_3O_8 groups made with
136 one TeO_4 and two TeO_{3+1} units with ZnO_{5+1} in octahedra-like structures between the chains.

137 Whereas, the ZnTeO_3 has Zn substituting Te to form new Zn-O-Te chains.

138 Pure ZnO crystal is made of chains of tetrahedra units.

139 By comparing each crystallized phases, it can be hypothesized that at low concentration of
140 ZnO, the zinc polyhedra could be between the tellurite chains in a pseudo-octahedral form
141 (looking like the $\text{Zn}_2\text{Te}_3\text{O}_8$ crystalline phase). And as ZnO content increases, the TeO_4 and
142 TeO_{3+1} polyhedra will decrease for an increase in TeO_3 polyhedra, the ZnO_{5+1} polyhedra will
143 also go toward a ZnO_{4+1} and will substitute the tellurium oxide inside the chains to form Te-O-
144 Zn bridges as shown in the ZnTeO_3 crystalline phase. It is possible that in glasses with high
145 concentration in zinc oxide, the ZnO will be tetrahedra-formed inside the chains (as shown in
146 the pure ZnO crystal). The crystallization of the samples have been presented elsewhere (33).

147 For an in-depth understanding of the vibration modes of the Raman spectroscopy of
 148 $Zn_2Te_3O_8$ and $ZnTeO_3$ crystalline phases, computational studies by using LADY software (34)
 149 were done, and a theoretical Raman spectra was calculated for each phases.



150
 151

Figure 2 : Simulated Raman spectra of the $Zn_2Te_3O_8$ and $ZnTeO_3$ crystalline phases

152 By comparing the Raman spectra of the two crystalline phases (figure 2), the evolution of
 153 the Raman spectra as a function of the concentration can be explained. An increase of ZnO
 154 content causes : (i) an increase of the Zn-O-Zn/Zn-O-Te bonds (300-400 cm^{-1}), (ii) a decrease
 155 of the Te -O-Te bridges (400-550 cm^{-1}), (iii) a decrease of TeO_4 polyhedra and an increase of
 156 TeO_3 polyhedra (550-800 cm^{-1}) is expected.

157 As the Boson peak (BP) is a manifestation of the excess of Vibrational Density of States
 158 (VDoS), phonon scattering is caused by intrinsic density fluctuations domains in the structure
 159 (within which short and medium range order is maintained and beyond which the material is
 160 isotropic). The BP, which is characteristic of the glassy state, will give important information
 161 allowing the correlation of the mechanical and structural approaches. This paper will focus on
 162 its evolution.

163
164

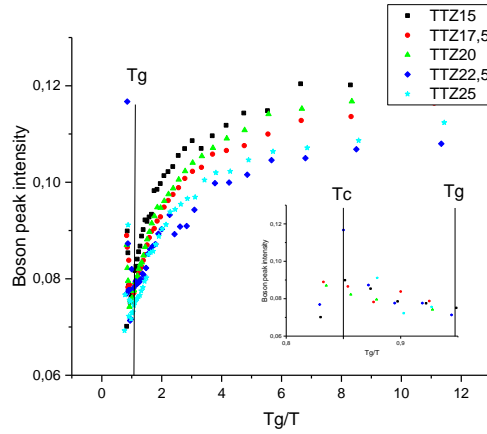
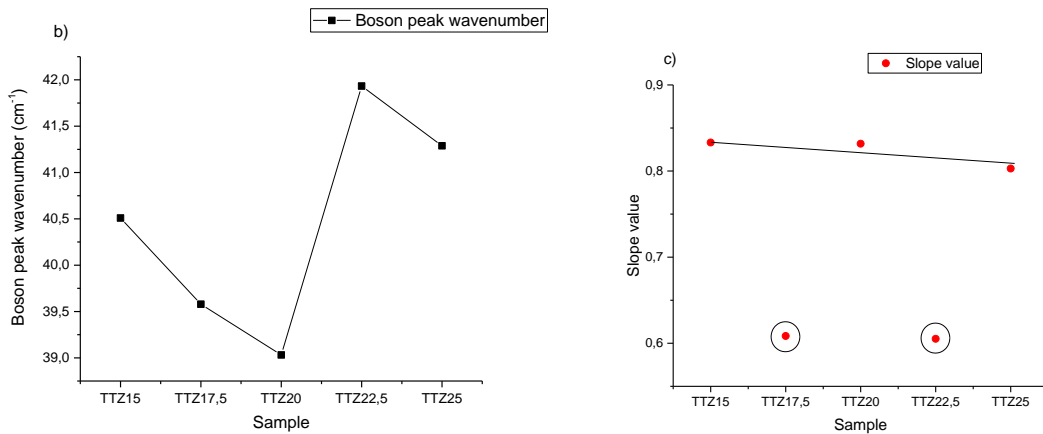
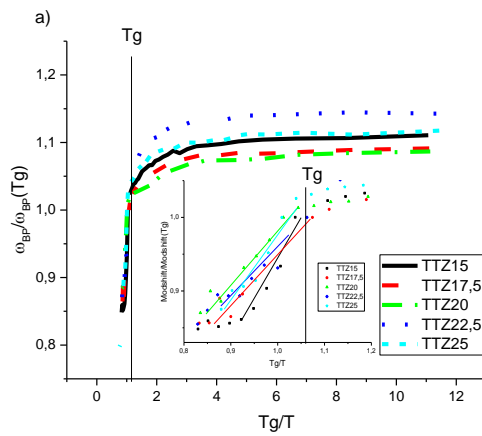


Figure 3: BP intensity as a function of T_g/T . Inset: zoom of the variations around T_g

165



166
167
168

Figure 4: **a)** ω_{BP} as a function of T_g/T . Inset: zoom of the variations around T_g **b)** ω_{BP} as a function of ZnO content at 30°C (RT). **c)** Average slope of data extracted from figure 4-a) after T_g

169 Most of the graphs will be presented in a non-conventional way, namely abscissa and
170 ordinate will be normalized by the value of the parameter under study at T_{gDSC} (obtained from
171 DSC measurements,) to facilitate the comparison between samples.

172 Figure 3 represents the evolution of the Boson peak (BP) intensity. A decrease of the BP
173 intensity before T_g is first observed and then followed by an increase up to crystallization
174 temperature.

175 Figure 4a, b, c summarized the Boson peak wavenumber evolution. Figure 4a illustrates the
 176 general evolution of the Boson peak wavenumber of each sample as a function of temperature.
 177 A slight shift to lower wavenumber up to Tg, and after this temperature, a strong difference of
 178 the wavenumber evolution is observed. Figure 4b shows the Boson peak wavenumber as a
 179 function of the composition at Room temperature (RT). A decrease of the wavenumber with an
 180 increase of the ZnO concentration is observed until TTZ20 and a strong increase of this intensity
 181 is noted for further concentrations. To illustrate the evolution of the Boson peak wavenumber
 182 after Tg, Figure 4c represents the evolution of the slope of the curve shown in Figure 4a; this
 183 slope represents the rate at which the wavenumber of the Boson peak is decreasing after Tg. A
 184 slight decrease of the value between TTZ15, TTZ20 and TTZ25 can be noted and an abnormal
 185 behavior compared to the previous three samples was observed for TTZ17.5 and TTZ22.5
 186 samples.

187 As a glass is considered composed of small domains with organized structure. Those
 188 domains (thereafter named blobs), are randomly arranged inside the glass, explaining its non-
 189 existent long order structuration.

190 When the BP intensity decreases, heterogeneity between blobs decreases (35,36). The
 191 present evolution means that with an increase in temperature, there is a rearrangement at short
 192 and intermediate distance of the glass to reach an energy minima at each temperature. After the
 193 glass transition temperature, the transition toward a viscous liquid will increase the
 194 heterogeneity of the glass. After the crystallization temperature, there is a decrease of intensity
 195 of the Boson peak due to the disappearance of the glass phase.

196 *Duval et al.* (37) and *Elliott et al.* (38) independently proposed a relationship between the
 197 size of the blobs ξ , the BP frequencies ω_{BP} and the mean sound velocities V_{av} (see equation 3)
 198 calculated from the mechanical properties of the glasses. The evolution of ω_{BP} then gives a first
 199 understanding of the evolution of the size of the blobs as a function of the temperature.

$$200 \quad \xi = V_{av}/\omega_{BP} \quad (1)$$

201 In the present study, before Tg, a classical trend as a function of temperature is observed, as
 202 glass is relaxing the size of the blobs increases, and after Tg, the samples goes toward a state of
 203 a viscous liquid, increasing the size even further (figure 4a).

204 Figure 4b evidences that at RT, ω_{BP} decreases up to TTZ20 and then increases meaning that
 205 blobs size firstly increases and then decreases.

206 ω_{BP} fluctuations clearly evidences a change in the structural behavior of the glass.

207 **2.2. Mechanical approach**

208 *2.2.1. RFDA*

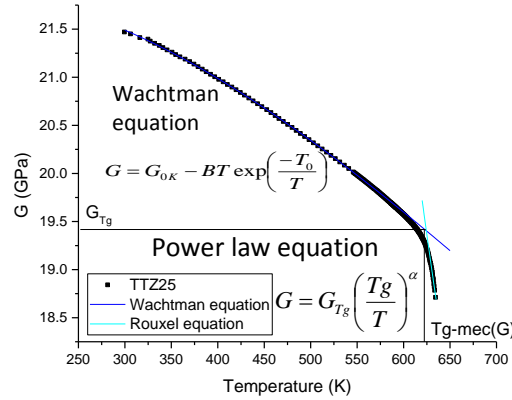
209 The temperature dependence of the elastic moduli and the shear moduli are illustrated figure
 210 8. As explained by *Mezeix et al.* (39) for silica glasses, a good description of the comportment
 211 of glasses at temperatures before Tg is obtained by using the model proposed by *Wachtman et*
 212 *al.* (40) (equation 2) and after Tg, this temperature dependence can be modeled by a power law
 213 equation proposed by *Rouxel et al.* (41) (equation 3).

$$214 \quad G = G_{0K} - BT \cdot \exp\left(\frac{-T_0}{T}\right) \quad (2)$$

$$215 \quad G = G_{Tg} \left(\frac{Tg}{T}\right)^\alpha \quad (3)$$

216 The obtained parameters of both simulated curves are reported on respectively table 2
 217 (Wachtman parameters) and table 3 (Rouxel parameters). The intersection of both calculated
 218 curves gives the value Tg. As this temperature is dependent of the thermal history of the sample,

219 this temperature will be denoted mechanical Tg: T_{gRFDA} . This T_{gRFDA} will be used to normalize
 220 the data.



221
 222 *Figure 5: Example of the shear modulus simulations as a function of temperature for the TTZ25 sample.*

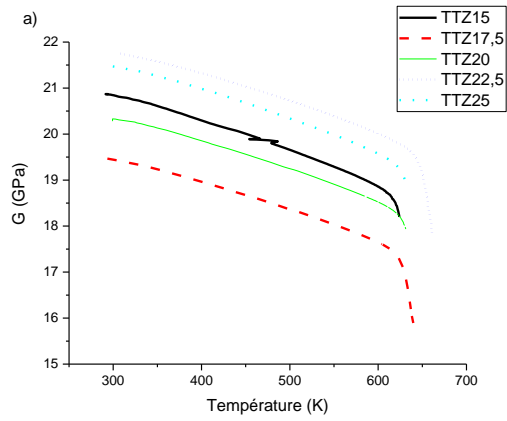
Sample	E			G		
	E_{0K}	B	T_0	G_{0K}	B	T_0
TTZ15	52.45	0.023	531	21.30	0.011	588
TTZ17.5	47.43	0.019	494	19.87	0.010	574
TTZ20	51.34	0.018	353	20.87	0.009	503
TTZ22.5	55.39	0.021	481	22.08	0.011	723
TTZ25	54.25	0.029	700	21.89	0.011	634

223 *Table 2 : Wachtman equation simulation parameters for E and G curves*

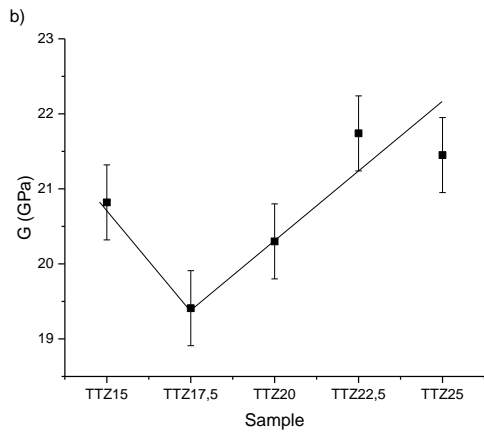
Sample	E			G		
	E_{Tg}	$Tg(E)$	α	G_{Tg}	$Tg(G)$	α
TTZ15	48.38	593	1.26	30.06	383	1.01
TTZ17.5	27.43	691	4.31	39.10	527	4.65
TTZ20	30.33	722	2.79	24.20	514	1.45
TTZ22.5	51.27	639	4.11	30.46	570	3.72
TTZ25	29.82	717	3.66	26.09	547	2.25

224 *Table 3 : Rouxel equation simulation parameters for E and G curves*

225 The B parameter of the Watchman equation is quite constant for both E and G data, which
 226 means that the evolution of the properties are equivalent up to T_g . On the opposite, the evolution
 227 of the simulated alpha coefficient from the Rouxel equation evidences huge variations which
 228 means that after T_g , Young and shear modulus have special trend which has to be studied.



229

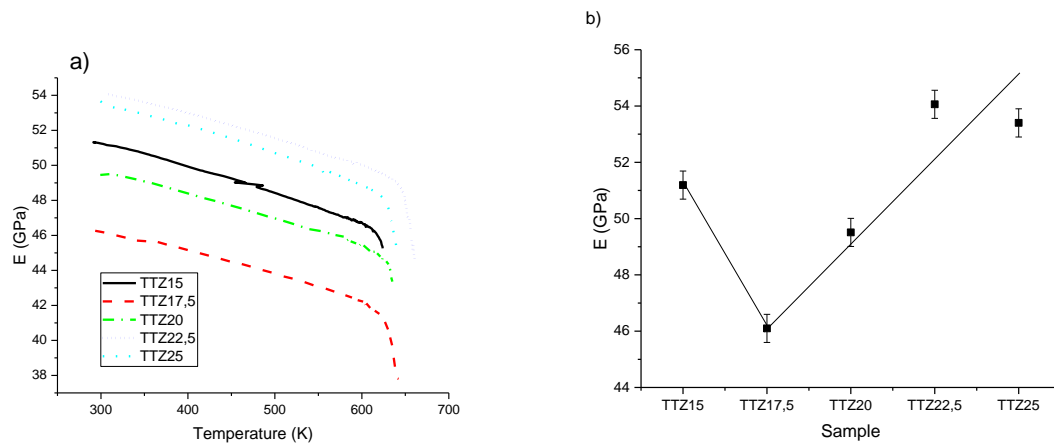


230

231

232

Figure 6: a) Shear modulus as a function of temperature in the TTZ_x ($x=15; 17.5; 20; 22.5; 25$) system. b) Shear modulus as a function of the concentration in ZnO at 30°C (RT)



233

234

235

Figure 7: a) Young modulus as a function of temperature in the TTZ_x ($x=15; 17.5; 20; 22.5; 25$) system. b) Young modulus as a function of the concentration in ZnO at RT

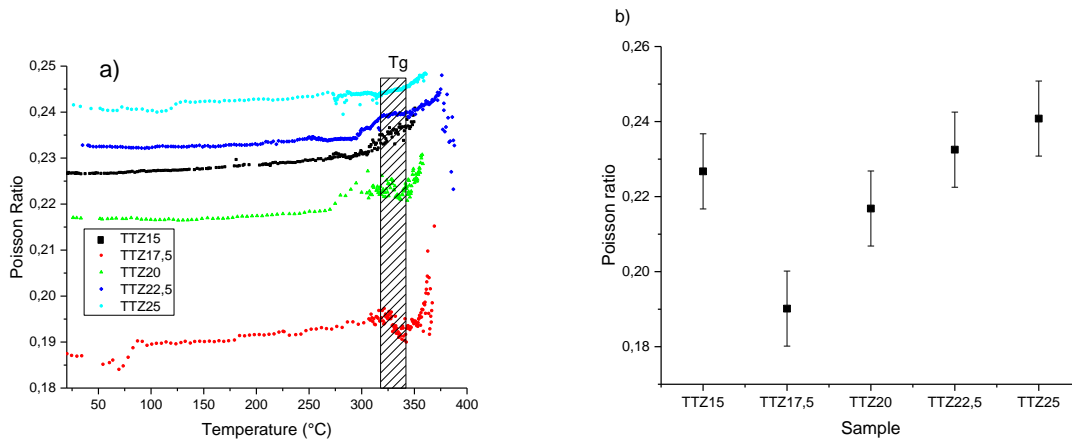


Figure 8: **a)** Evolution of the Poisson ratio as a function of temperature. **b)** Evolution of the Poisson ratio as a function of the glass composition at RT

236
237
238

239 As a function of temperature, for each sample, a slight decrease of E and G before T_g is observed which is exacerbated after (figure 6a and 7a). The Poisson ratio, which is calculated using G and E, presents also strong variations around T_g (figure 8a). This evolution will be further discussed in the discussion part.

243 The evolution of the E, G and ν values (figure 6b, 7b, 8b respectively) at room temperature and as a function of the concentration show an equivalent variation: a decrease of their values from TTZ15 to TTZ17.5 and then an increase from TTZ17.5 to TTZ25 is observed. Those results are consistent with the results previously published by Ghribi *et al.* (33), using ultrasonic echography experiments.

248 As Poisson ratio gives an information on the average connectivity of the glass (42), an increase of the connectivity of the network before TTZ17.5 and a decrease of the connectivity after is observed. Those results are consistent with the proposed theory: at low concentration of ZnO, Zinc oxide polyhedra are localized between the tellurite chains, linking them together by weak bonding, increasing by consequence the connectivity of the network but decreasing E and G values. At higher concentration, zinc atom substitutes Te atom within the chains, so it does not link the chains as it did at lower concentration. This in turn will decrease the connectivity of the network and increase once more E and G values compared to the lower concentration of zinc oxide.

257 The alpha coefficient (extracted from the Power law equation), which expresses the softening rate and which is correlated to the liquid fragility index (39), was calculated by measuring the slope of the curve obtained after plotting $\log(G/G(T_g))$ versus $f(\log(T_g/T))$ for temperatures higher than T_g (figure 9a). The same way is used for $\log(E/E(T_g))=f(\log T_g/T)$ (figure 9b).

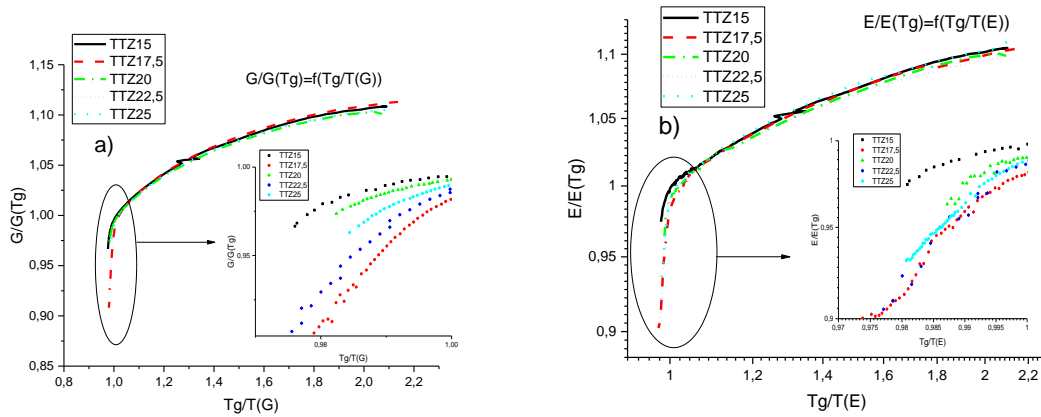
262 The α coefficient evolution as a function of the concentration (figure 10) shows that the two glasses with the highest α value are the TTZ17.5 and TTZ22.5 samples. The other three glasses have a linear increase of the α coefficient value.

265 An higher value of α coefficient means a higher rate of decreasing mechanical properties, so the linear increase in the α coefficient value between TTZ15, TTZ20 and TTZ22.5 glasses means that the more ZnO content inside the glass, the faster the mechanical properties will decrease after T_g. The α coefficient for the two glasses TTZ17.5 and TTZ22.5 shows that the mechanical properties of these two glasses decrease at a faster rate.

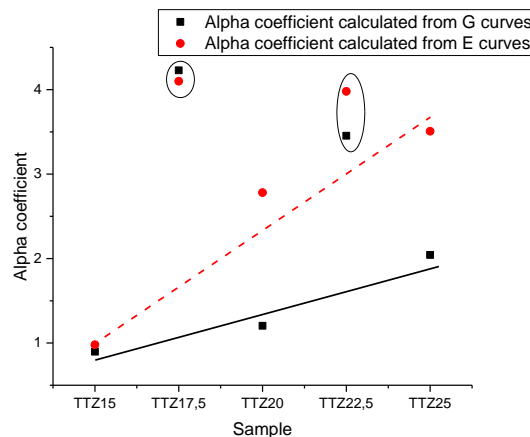
269

270 Comparing the evolution of the TTZ17.5 glass to the previous conclusion on the structural
 271 properties, another hypothesis can be added: when the Zinc oxide is between the tellurite chains,
 272 the bonds between the Zinc oxide and the tellurium oxide are weak, and become even weaker
 273 after the glass transition temperature (decreasing at the same time the mechanical properties
 274 faster (higher α coefficient value)).

275 The evolution of the TTZ22.5 glass sample is still under study and other experiments are
 276 being done to understand the strange behavior of this sample compared to other compositions.



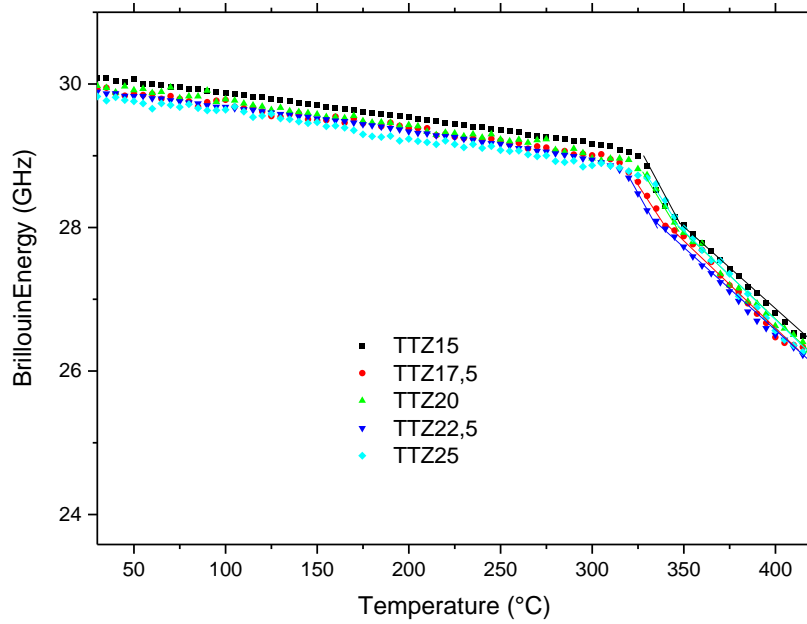
277
 278 **Figure 9: a) $G/G(T_g)=f(T_g/T)$; b) $E/E(T_g)=f(T_g/T)$; Insets: zoom of the variations around T_g**



279
 280 **Figure 10 : Alpha coefficient as a function of the ZnO concentration**

281 2.2.2. ARABICA experiment

282 In the Brillouin spectra, due to the backscattering geometry used in the experimental setup
 283 only longitudinal mode are observed. The position of the Brillouin band strongly depends on
 284 the temperature (figure 11). A slight shift of the Brillouin position to lower energy before the
 285 glass transition temperature (T_{gDSC}) is observed. Around 20°C before the glass transition
 286 temperature, a sharper decrease of the Brillouin shift is observed followed by a second slope
 287 break. The variation just before the glass transition temperature will be further discussed in the
 288 discussion part.

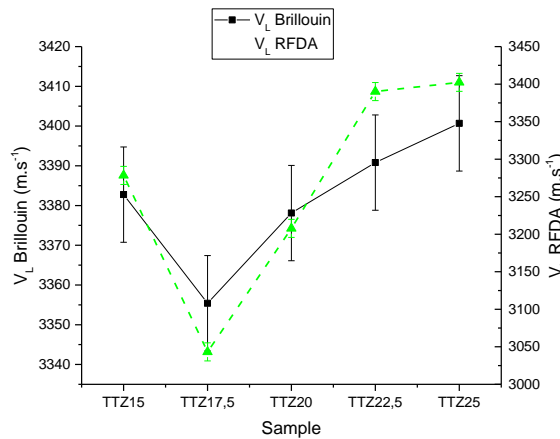


289
290 *Figure 11: TTZ glasses Brillouin position as a function of temperature*

291 As the Brillouin shift is proportional to the longitudinal velocity of the glasses, so
292 proportional to the mechanical properties of each samples (equation 4). It is then possible to
293 compare the mechanical properties obtained by RFDA experiments to the results from the
294 Brillouin shift.

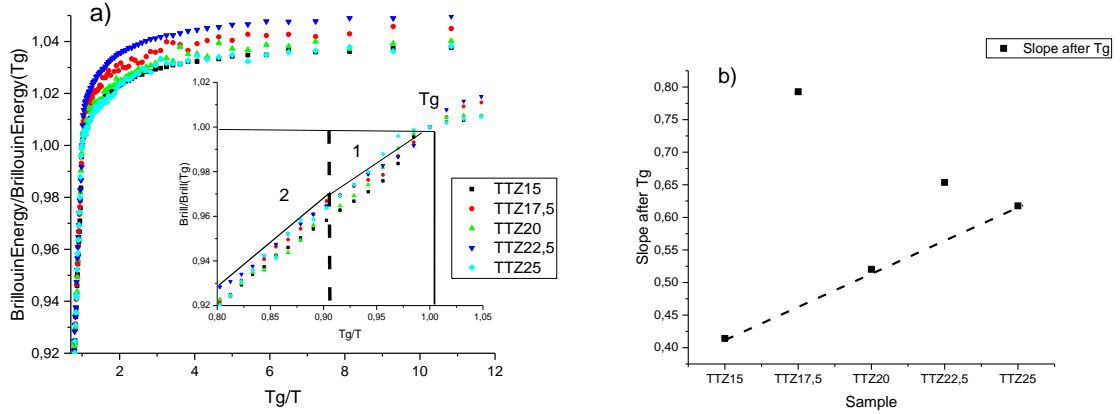
295
$$V_L(\text{Brillouin}) = \frac{\lambda(\text{Brillouin shift})}{2n} \quad (4)$$

296 With λ the wavelength of the measurement (488nm in this work) and n the linear refractive
297 index at the same wavelength.



298
299 *Figure 12: Variation of the longitudinal velocities calculated from the Brillouin and RFDA experiments as a*
300 *function of the concentration in zinc oxide at room temperature.*

301 Thanks to the figure 12, which compare the variation of the longitudinal velocities obtained
302 by Brillouin experiment and RFDA experiment as a function of the ZnO content, a good
303 agreement of the variation is found between the two different techniques, with a decrease of the
304 longitudinal velocities between TTZ15 and TTZ17.5 followed by an increase thereafter.



305
306 *Figure 13: a) Brillouin peak energy normalized with the Brillouin peak energy at the glass transition*
307 *temperature as a function of Tg/T. Inset: zoom of the variations around Tg b) Variation of the slope in the*
308 *second regime after the glass transition temperature*

309 By normalizing the Brillouin shift in the same way as for the mechanical properties to extract
310 the alpha coefficient of the power law equation, it is possible to compare the evolution of the
311 mechanical properties and the variation of the Brillouin energy by calculating the slopes in the
312 second part of the graphic in figure 13a.

313 Hence, by comparing the values of slope calculated showed in figure 13b to the one from
314 the α coefficient (figure 10), it is shown that the evolution as a function of the concentration has
315 the same linear evolution between the three samples TTZ15, TTZ20 and TTZ25 with two
316 anomalies being TTZ17.5 and TTZ22.5.

317 The results of the Brillouin experiment are in a good agreement with the mechanical
318 properties as a function of the concentration but also as a function of temperature, with a slight
319 decrease of the Brillouin shift as the mechanical properties decrease, and so even after Tg.

320 2.3. Discussion

321

Sample	Tg _{Raman} (°C) (±10°C)	Tg _{RFDA} (°C)		Tg _{Brillouin} (°C) (±10°C)	Tg _{DSC} (°C) (±5°C)
		Tg(E) (±5°C)	Tg(G) (±5°C)		
TTZ15	310	339	336	336	335
TTZ17.5	313	353	354	339	337
TTZ20	321	354	347	341	339
TTZ22.5	324	372	372	340	341
TTZ25	331	355	351	345	343

322 *Table 4 : Glass temperature measured by the different experiments (The values of Tg_{DSC} shown in table 3 were*
323 *measured thanks to the ARABICA setup at the same time as the Brillouin shift measures).*

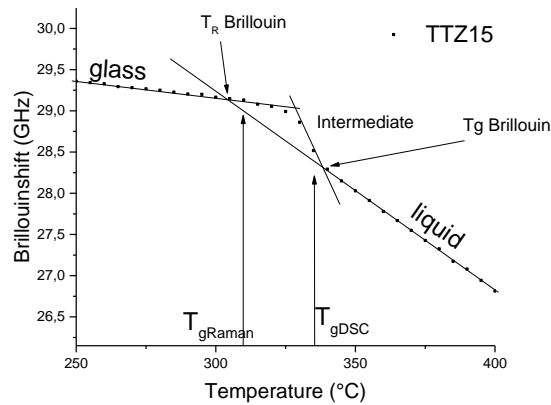
324 A first interesting comment can be done on the difference between the values of Tg obtained
325 as a function of the technique used. Using the same method as for RFDA data to extract a
326 mechanical Tg, Raman data have been fitted with linear functions before and after the slope
327 break observed on data, the value of Tg is extracted at the intersection of the two fitted parts.
328 Comparing Tg_{Raman} and Tg_{RFDA} to Tg_{DSC}, it can be seen that Tg_{Raman} is lower and Tg_{RFDA} is
329 higher. This difference partly come from the difference of sample's size, the difference of the
330 heating rate (5°C/min for Raman spectroscopy and 10°C/min for the RFDA and ARABICA

331 measurements). Moreover Raman data are obtained in a semi-dynamic way (Stop of the heating
 332 ramp during acquisition time) and not a dynamic one like RFDA and ARABICA data recording.
 333

334 Now, looking at Brillouin and RFDA experiments (in particular the Poisson coefficient)
 335 more in details, some interesting facts can be noted:

336 In Brillouin experiment (figure 11), Brillouin shift evolution exhibits an intermediate slope
 337 break between the glassy state and the liquid one: This intermediate domain is characteristic of
 338 relaxation events suggesting that the heating rate of 10°C/min used for the experiment was too
 339 fast, creating strains inside the glass. The intercept between the intermediate and the liquid part
 340 is equivalent to the T_{gDSC} and was used to define the $T_{gBrillouin}$ (results shown on table 4).

341 By comparing the Brillouin data to the Raman data it can be noticed in Figure 14 that the
 342 T_{gRaman} corresponds to the intercept of the linear extrapolation between the glassy state and the
 343 liquid one of the Brillouin shift (relaxation temperature (T_R) values in table 5). This also
 344 corresponds to the strong variation around T_g found on the Poisson ratio curve (figure 9), where
 345 the variation in Poisson ratio starts to fluctuate (values in table 5). This means that the relaxation
 346 of the sample due to the high heating rate will strongly affect the connectivity of the network
 347 before the glass transition temperature, due to a rearrangement of the glassy network.



348
 349 Figure 14 : Example of how the relaxation temperature and the glass transition temperature are obtained
 350 (TTZ15 glass)

351

Sample	T_R Brillouin (°C)	T_R RFDA (°C)
TTZ15	303	305
TTZ17.5	307	306
TTZ20	312	309
TTZ22.5	307	301
TTZ25	322	316

352 Table 5 : Relaxation temperatures for each samples in RFDA and Brillouin experiments

353 To go further, as explained before, *Duval et al.* (37) and *Elliott et al.* (38) independently
 354 found a relationship that links the size of density fluctuations domains ξ with the position of the
 355 Boson peak frequency ω_{BP} and the sound velocities inside the glasses.

356
$$\xi = \frac{V_{av}}{\omega_{BP}} \quad (3)$$

357 With V_{av} the average between the transversal velocity (V_T) and the longitudinal velocity
 358 (V_L). It is possible to calculate the two required velocities with the two equation below

386
387

$$V_T = \sqrt{\frac{G}{\rho}} \quad V_L = \sqrt{\frac{K + \frac{4G}{3}}{\rho}} \quad K = \frac{1}{3} \cdot \frac{E}{1 - 2\nu} \quad (4)$$

With K the Bulk modulus. V_{av} is then calculated with the equation below.

388

$$V_{av} = \left(\frac{1}{3V_l^3} + \frac{2}{3V_t^3} \right)^{-1/3} \quad (5)$$

389

Figure 15a represents the evolution of the size of the domains as a function of temperature. Before the glass transition temperature, a slight increase of this parameter is evidenced, with a steeper increase after the glass transition temperature. This evolution is in accordance to the previous evolution of the Boson Peak, and correspond to the relaxation of the glass before Tg and then the transition toward a viscous liquid after Tg.

394

As a function of the concentration (Figure 15b), two different evolutions can be seen: a sharp decrease of the size of the blobs between TTZ15 and TTZ17.5 and hereafter data are almost constant. This means that drastic changes of the structure after TTZ17.5 are observed, which can be explained by the change of the Zn atom coordination number as a function of ZnO content.

399

The discrepancy between the evolution of the size of the blobs as a function of the concentration and the evolution of the Boson peak wavenumber comes from the evolution of the sound velocities, and by this bias the evolution of the mechanical properties. This also means that having the Boson peak wavenumber evolution isn't enough to understand exactly how the size of the blobs evolve, even if it can give a rough understanding of this evolution as shown as a function of temperature.

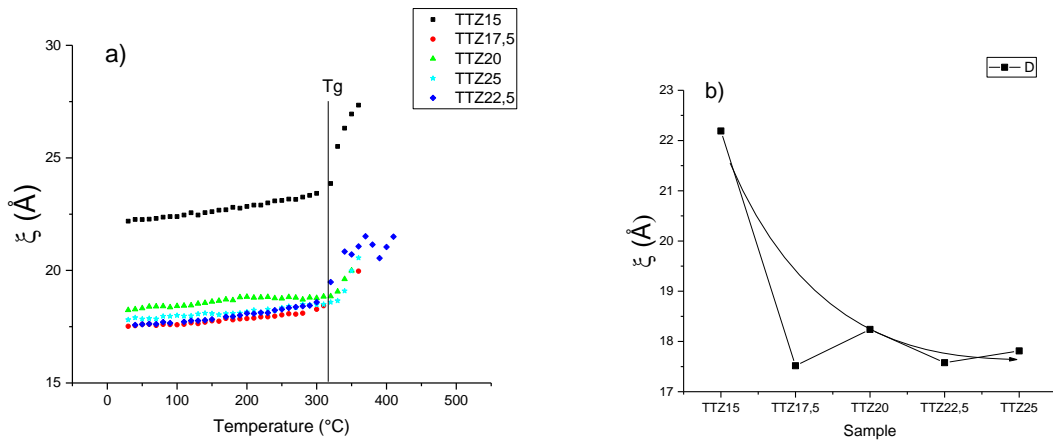
400

401

402

403

404



405

406

407

Figure 15 : Evolution of the size of the blobs as a function of a) temperature; b) the concentration in ZnO (at RT)

408 3. Conclusion

409

Correlation between structural properties of glasses to different kind of macroscopic physic one has been one of the most important field of research on glasses for years. In this study, some interesting facts have been pointed out.

412

By comparing RFDA experiments and Raman spectroscopy, it has been possible to understand the structural properties of a glass having a complex structure with two entities that have a coordination number which change as a function of the TeO₂ and ZnO content. (i) As usual Raman spectroscopy gave informations on the change of the Te-O polyedra inside the

415

416 glass, (ii) RFDA experiment gave an understanding on the strength of the different bonds as a
417 function of the concentration, and (iii) from both Raman and RFDA experiments by calculating
418 the blobs size, the structural evolution of the glass at intermediate-distance has been evidenced.

419 Lastly, the behavior of the samples after the glass transition temperature has been evidenced
420 and links to the particular behavior of Zinc polyhedra were noted. Indeed, the variation of the
421 alpha coefficient of the mechanical properties studied by RFDA experiment, the variation of
422 the slope after T_g of the Brillouin experiment and the variation of the slope of the shift in
423 wavenumber of the Boson peak recorded in Raman spectroscopy, some anomalies stood out
424 exactly at the same ZnO content : 17.5%ZnO and 22.5%ZnO.

425 Concerning mechanical properties, a higher slope value after the glass transition means that
426 the decrease of the mechanical properties is faster

427 In Raman spectroscopy, a shift toward lower wavenumber means that the blobs size
428 increases. So a higher slope value after the glass transition means that the blobs size increases
429 at a higher rate.

430 From the two previous point, it can be porposed that: when the blobs size increase at a faster
431 rate, the mechanical properties will decrease at a slower rate. Thanks to this hypothesis, it will
432 be easier to predict how the mechanical properties will evolve at temperature close and higher
433 than T_g which will be helpful for optical fiber shaping.

434 4. Acknowledgement

435 The authors thank Dr. J. Cornette for valued assistance with Raman experiments and O.
436 Noguera for his help on Raman spectra simulation. J. de CLERMONT-GALLERANDE also
437 gratefully acknowledges the financial support from Conseil Régional du Limousin and the
438 PICS.

439 Bibliography

- 440 [1] R. A. H. El-Mallawany, *Tellurite glasses handbook: physical properties and data*, 2nd ed.
441 Boca Raton, FL: Taylor & Francis, 2011.
- 442 [2] A. P. Mirgorodsky, M. Soulis, P. Thomas, T. Merle-Méjean, and M. Smirnov, “*Ab initio*
443 study of the nonlinear optical susceptibility of Te O 2 -based glasses,” *Phys. Rev. B*, vol.
444 73, no. 13, Apr. 2006.
- 445 [3] J. S. Wang, E. M. Vogel, and E. Snitzer, “Tellurite glass: a new candidate for fiber
446 devices,” *Opt. Mater.*, vol. 3, no. 3, pp. 187–203, Aug. 1994.
- 447 [4] S.-H. Kim, T. Yoko, and S. Sakka, “Linear and Nonlinear Optical Properties of TeO₂
448 Glass,” *J. Am. Ceram. Soc.*, vol. 76, no. 10, pp. 2486–2490, Oct. 1993.
- 449 [5] M. Soulis *et al.*, “Local molecular orbitals and hyper-susceptibility of TeO₂ glass,” *J. Non-*
450 *Cryst. Solids*, vol. 354, no. 2–9, pp. 199–202, Jan. 2008.
- 451 [6] J.-R. Duclère *et al.*, “Third order nonlinear optical properties of a paratellurite single
452 crystal,” *J. Appl. Phys.*, vol. 123, no. 18, p. 183105, May 2018.
- 453 [7] P. T. Sarjeant and R. Roy, “New Glassy and Polymorphic Oxide Phases Using Rapid
454 Quenching Techniques,” *J. Am. Ceram. Soc.*, vol. 50, no. 10, pp. 500–503, Oct. 1967.
- 455 [8] M. Udovic *et al.*, “Thermal characteristics, Raman spectra and structural properties of new
456 tellurite glasses within the Bi₂O₃–TiO₂–TeO₂ system,” *J. Solid State Chem.*, vol. 179,
457 no. 10, pp. 3252–3259, Oct. 2006.
- 458 [9] M. Udovic *et al.*, “Formation domain and characterization of new glasses within the Ti₂O–
459 TiO₂–TeO₂ system,” *Mater. Res. Bull.*, vol. 44, no. 2, pp. 248–253, Feb. 2009.

- 460 [10] D. Linda *et al.*, “New glasses within the $\text{Ti}_2\text{O}-\text{Ag}_2\text{O}-\text{TeO}_2$ system: Thermal
461 characteristics, Raman spectra and structural properties,” *Mater. Res. Bull.*, vol. 45, no.
462 12, pp. 1816–1824, Dec. 2010.
- 463 [11] O. Noguera, T. Merle-Méjean, A. P. Mirgorodsky, P. Thomas, and J.-C. Champarnaud-
464 Mesjard, “Dynamics and crystal chemistry of tellurites. II. Composition- and temperature-
465 dependence of the Raman spectra of $x(\text{Ti}_2\text{O})+(1-x) \text{Te}_2\text{O}$ glasses: evidence for a phase
466 separation?,” *J. Phys. Chem. Solids*, vol. 65, no. 5, pp. 981–993, May 2004.
- 467 [12] M. Dutreilh-Colas, P. Charton, P. Thomas, P. Armand, P. Marchet, and J. C.
468 Champarnaud-Mesjard, “The TeO_2 -rich part of the $\text{TeO}_2-\text{Ga}_2\text{O}_3$ system: equilibrium
469 and non-equilibrium phase diagram,” *J Mater Chem*, vol. 12, no. 9, pp. 2803–2806, 2002.
- 470 [13] S. Blanchandin, P. Thomas, P. Marchet, J. C. Champarnaud-Mesjard, and B. Frit, “New
471 heavy metal oxide glasses: investigations within the $\text{TeO}_2-\text{Nb}_2\text{O}_5-\text{Bi}_2\text{O}_3$ system,” *J.*
472 *Alloys Compd.*, vol. 347, no. 1–2, pp. 206–212, Dec. 2002.
- 473 [14] B. Jeansannetas *et al.*, “Glass Structure and Optical Nonlinearities in Thallium(I)
474 Tellurium(IV) Oxide Glasses,” *J. Solid State Chem.*, vol. 146, no. 2, pp. 329–335, Sep.
475 1999.
- 476 [15] M. Soulis, A. P. Mirgorodsky, T. Merle-Méjean, O. Masson, P. Thomas, and M. Udovic,
477 “The role of modifier’s cation valence in structural properties of TeO_2 -based glasses,” *J.*
478 *Non-Cryst. Solids*, vol. 354, no. 2–9, pp. 143–149, Jan. 2008.
- 479 [16] M. R. Zaki, D. Hamani, M. Dutreilh-Colas, J.-R. Duclère, O. Masson, and P. Thomas,
480 “Synthesis, thermal, structural and linear optical properties of new glasses within the
481 $\text{TeO}_2-\text{TiO}_2-\text{WO}_3$ system,” *J. Non-Cryst. Solids*, vol. 484, pp. 139–148, Mar. 2018.
- 482 [17] S. kareem Ahmmad, M. A. Samee, A. Edukondalu, and S. Rahman, “Physical and optical
483 properties of zinc arsenic tellurite glasses,” *Results Phys.*, vol. 2, pp. 175–181, 2012.
- 484 [18] L. G. Van Uitert and S. H. Wemple, “ ZnCl_2 glass: A potential ultralow-loss optical fiber
485 material,” *Appl. Phys. Lett.*, vol. 33, no. 1, pp. 57–59, Jul. 1978.
- 486 [19] T. Sekiya, N. Mochida, and A. Ohtsuka, “Raman spectra of $\text{MO}-\text{TeO}_2$ ($\text{M} = \text{Mg}, \text{Sr}, \text{Ba}$
487 and Zn) glasses,” *J. Non-Cryst. Solids*, vol. 168, no. 1–2, pp. 106–114, Feb. 1994.
- 488 [20] H. Bürger, K. Kneipp, H. Hobert, W. Vogel, V. Kozhukharov, and S. Neov, “Glass
489 formation, properties and structure of glasses in the TeO_2-ZnO system,” *J. Non-Cryst.*
490 *Solids*, vol. 151, no. 1–2, pp. 134–142, Dec. 1992.
- 491 [21] C. Duverger, M. Bouazaoui, and S. Turrell, “Raman spectroscopic investigations of the
492 effect of the doping metal on the structure of binary tellurium-oxide glasses,” *J. Non-*
493 *Cryst. Solids*, vol. 220, no. 2–3, pp. 169–177, Nov. 1997.
- 494 [22] U. Hoppe, E. Yousef, C. Rüssel, J. Neuefeind, and A. C. Hannon, “Structure of zinc and
495 niobium tellurite glasses by neutron and x-ray diffraction,” *J. Phys. Condens. Matter*, vol.
496 16, no. 9, p. 1645, 2004.
- 497 [23] V. Kozhukharov, H. Bürger, S. Neov, and B. Sidzhimov, “Atomic arrangement of a zinc-
498 tellurite glass,” *Polyhedron*, vol. 5, no. 3, pp. 771–777, Jan. 1986.
- 499 [24] J. G. Thorbahn and J. W. Zwanziger, “Compositional dependence of the stress-optic
500 response in zinc tellurite glasses,” *J. Non-Cryst. Solids*, vol. 381, pp. 48–53, Dec. 2013.
- 501 [25] N. Ghribi *et al.*, “Thermal, optical and structural properties of glasses within the
502 $\text{TeO}_2\text{TiO}_2\text{ZnO}$ system,” *J. Alloys Compd.*, vol. 622, pp. 333–340, Feb. 2015.
- 503 [26] ASTM International, “Standard Test Method for Dynamic Young’s Modulus, Shear
504 Modulus and Poisson’s Ratio by Impulse Excitation of Vibration.” ASTM E1876- 01,
505 2006.
- 506 [27] I. Kabalci, N. Ö. Körpe, T. Duran, and M. Özdemir, “Optical properties and crystallization
507 kinetics of $(\text{TeO}_2)(\text{ZnO})(\text{TiO}_2)$ glasses: Optical properties and crystallization kinetics of
508 $(\text{TeO}_2)(\text{ZnO})(\text{TiO}_2)$ glasses,” *Phys. Status Solidi C*, vol. 8, no. 9, pp. 2629–2632, Sep.
509 2011.

- 510 [28] D. de Sousa Menses, *FOCUS version 1.0, software utility for the creation of optical*
511 *function.* .
- 512 [29] N. Ghribi *et al.*, “Structural, mechanical and optical investigations in the TeO₂-rich part
513 of the TeO₂-GeO₂-ZnO ternary glass system,” *Solid State Sci.*, vol. 40, pp. 20–30, Feb.
514 2015.
- 515 [30] A. Veber, M. R. Cicconi, H. Reinfelder, and D. de Ligny, “Combined Differential
516 scanning calorimetry, Raman and Brillouin spectroscopies: A multiscale approach for
517 materials investigation,” *Anal. Chim. Acta*, vol. 998, pp. 37–44, Jan. 2018.
- 518 [31] K. Hanke, “Die Kristallstruktur von Zn₂Te₃O₈,” *Naturwissenschaften*, vol. 53, no. 11, pp.
519 273–273, 1966.
- 520 [32] K. Hanke, “Zinktellurit: Kristallstruktur und Beziehungen zu einigen Seleniten,”
521 *Naturwissenschaften*, vol. 54, no. 8, pp. 199–199, 1967.
- 522 [33] N. Ghribi, *Synthesis, structural and mechanical investigations of new tellurite materials*
523 *for non-linear optical applications*. Limoges, 2015.
- 524 [34] M. B. Smirnov and V. Y. Kazimirov, “LADY: Software for lattice dynamics simulations,”
525 *JINR Commun.*, vol. E14, p. 159, 2001.
- 526 [35] E. Duval *et al.*, “Inelastic light, neutron, and X-ray scattering related to the heterogeneous
527 elasticity of glasses,” *J. Non-Cryst. Solids*, vol. 307–310, pp. 103–108, Sep. 2002.
- 528 [36] B. Champagnon, L. Wondraczek, and T. Deschamps, “Boson peak, structural
529 inhomogeneity, light scattering and transparency of silicate glasses,” *J. Non-Cryst. Solids*,
530 vol. 355, no. 10–12, pp. 712–714, May 2009.
- 531 [37] E. Duval, A. Boukenter, and T. Achibat, “Vibrational dynamics and the structure of
532 glasses,” *J. Phys. Condens. Matter*, vol. 2, no. 51, pp. 10227–10234, Dec. 1990.
- 533 [38] S. R. Elliott, “A Unified Model for the Low-Energy Vibrational Behaviour of Amorphous
534 Solids,” *Europhys. Lett. EPL*, vol. 19, no. 3, pp. 201–206, Jun. 1992.
- 535 [39] P. Mezeix, F. Célarié, P. Houizot, Y. Gueguen, F. Muñoz, and T. Rouxel, “Elasticity and
536 viscosity of BaO-TiO₂-SiO₂ glasses in the 0.9 to 1.2Tg temperature interval,” *J. Non-*
537 *Cryst. Solids*, vol. 445–446, pp. 45–52, Aug. 2016.
- 538 [40] J. B. Wachtman, W. E. Tefft, D. G. Lam, and C. S. Apstein, “Exponential Temperature
539 Dependence of Young’s Modulus for Several Oxides,” *Phys. Rev.*, vol. 122, no. 6, pp.
540 1754–1759, Jun. 1961.
- 541 [41] T. Rouxel, “Elastic Properties and Short-to Medium-Range Order in Glasses,” *J. Am.*
542 *Ceram. Soc.*, vol. 90, no. 10, pp. 3019–3039, Oct. 2007.
- 543 [42] G. N. Greaves, A. L. Greer, R. S. Lakes, and T. Rouxel, “Poisson’s ratio and modern
544 materials,” *Nat. Mater.*, vol. 10, no. 11, pp. 823–837, Nov. 2011.
- 545